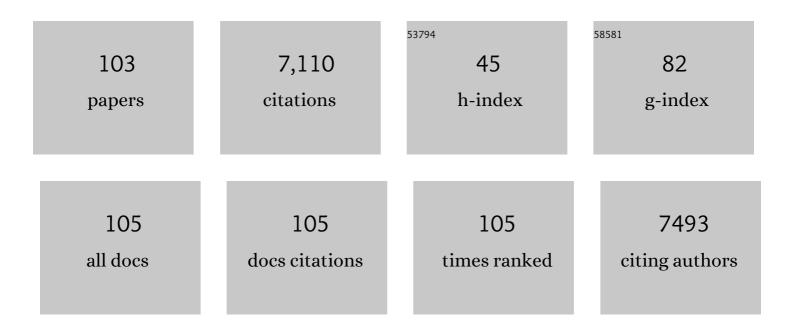
List of Publications by Year in descending order

Source: https://exaly.com/author-pdf/5640570/publications.pdf Version: 2024-02-01



YANG PENG

#	Article	IF	CITATIONS
1	Methane Storage in Metal–Organic Frameworks: Current Records, Surprise Findings, and Challenges. Journal of the American Chemical Society, 2013, 135, 11887-11894.	13.7	841
2	High-performance lithium sulfur batteries enabled by a synergy between sulfur and carbon nanotubes. Energy Storage Materials, 2019, 16, 194-202.	18.0	264
3	A hierarchical nickel–carbon structure templated by metal–organic frameworks for efficient overall water splitting. Energy and Environmental Science, 2018, 11, 2363-2371.	30.8	240
4	Carved nanoframes of cobalt–iron bimetal phosphide as a bifunctional electrocatalyst for efficient overall water splitting. Chemical Science, 2019, 10, 464-474.	7.4	238
5	Morphological and Electronic Tuning of Ni ₂ P through Iron Doping toward Highly Efficient Water Splitting. ACS Catalysis, 2019, 9, 8882-8892.	11.2	227
6	Reaction of Hydrogen or Ammonia with Unsaturated Germanium or Tin Molecules under Ambient Conditions: Oxidative Addition versus Arene Elimination. Journal of the American Chemical Society, 2009, 131, 16272-16282.	13.7	218
7	Diarylstannylene Activation of Hydrogen or Ammonia with Arene Elimination. Journal of the American Chemical Society, 2008, 130, 12268-12269.	13.7	206
8	Unpaired 3d Electrons on Atomically Dispersed Cobalt Centres in Coordination Polymers Regulate both Oxygen Reduction Reaction (ORR) Activity and Selectivity for Use in Zinc–Air Batteries. Angewandte Chemie - International Edition, 2020, 59, 286-294.	13.8	200
9	Topotactically Transformed Polygonal Mesopores on Ternary Layered Double Hydroxides Exposing Underâ€Coordinated Metal Centers for Accelerated Water Dissociation. Advanced Materials, 2020, 32, e2006784.	21.0	186
10	Reversible Reactions of Ethylene with Distannynes Under Ambient Conditions. Science, 2009, 325, 1668-1670.	12.6	185
11	Electrostatic charge transfer for boosting the photocatalytic CO2 reduction on metal centers of 2D MOF/rGO heterostructure. Applied Catalysis B: Environmental, 2020, 262, 118144.	20.2	175
12	Selective reduction of CO2 by conductive MOF nanosheets as an efficient co-catalyst under visible light illumination. Applied Catalysis B: Environmental, 2018, 238, 339-345.	20.2	166
13	Addition of H2 to distannynes under ambient conditions. Chemical Communications, 2008, , 6042.	4.1	147
14	Atomic Ir-doped NiCo layered double hydroxide as a bifunctional electrocatalyst for highly efficient and durable water splitting. Journal of Materials Chemistry A, 2020, 8, 9871-9881.	10.3	144
15	Simultaneously high gravimetric and volumetric methane uptake characteristics of the metal–organic framework NU-111. Chemical Communications, 2013, 49, 2992.	4.1	137
16	Addition of Hydrogen or Ammonia to a Lowâ€Valent Groupâ€13 Metal Species at 25 °C and 1â€Atmos Angewandte Chemie - International Edition, 2009, 48, 2031-2034.	phere. 13.8	126
17	Visible-Light Photocatalytic CO ₂ Reduction Using Metal-Organic Framework Derived Ni(OH) ₂ Nanocages: A Synergy from Multiple Light Reflection, Static Charge Transfer, and Oxygen Vacancies. ACS Catalysis, 2021, 11, 345-354.	11.2	117
18	Geometric Modulation of Local CO Flux in Ag@Cu ₂ O Nanoreactors for Steering the CO ₂ RR Pathway toward Highâ€Efficacy Methane Production. Advanced Materials, 2021, 33, e2101741.	21.0	116

YANG PENG

#	Article	IF	CITATIONS
19	Carborane-Based Metal–Organic Framework with High Methane and Hydrogen Storage Capacities. Chemistry of Materials, 2013, 25, 3539-3543.	6.7	115
20	Substituent effects in ditetrel alkyne analogues: multiple vs. single bonded isomers. Chemical Science, 2010, 1, 461.	7.4	113
21	Octahedral gold-silver nanoframes with rich crystalline defects for efficient methanol oxidation manifesting a CO-promoting effect. Nature Communications, 2019, 10, 3782.	12.8	113
22	Anchoring MOF-derived CoS ₂ on sulfurized polyacrylonitrile nanofibers for high areal capacity lithium–sulfur batteries. Journal of Materials Chemistry A, 2020, 8, 1298-1306.	10.3	112
23	Isomeric Forms of Heavier Main Group Hydrides:  Experimental and Theoretical Studies of the [Sn(Ar)H]2 (Ar = Terphenyl) System. Journal of the American Chemical Society, 2007, 129, 16197-16208.	13.7	102
24	Phase and Morphology Transformation of MnO ₂ Induced by Ionic Liquids toward Efficient Water Oxidation. ACS Catalysis, 2018, 8, 10137-10147.	11.2	102
25	In situ construction of CoSe2@vertical-oriented graphene arrays as self-supporting electrodes for sodium-ion capacitors and electrocatalytic oxygen evolution. Nano Energy, 2019, 60, 385-393.	16.0	93
26	Breaking the Linear Scaling Relationship by Compositional and Structural Crafting of Ternary Cu–Au/Ag Nanoframes for Electrocatalytic Ethylene Production. Angewandte Chemie - International Edition, 2021, 60, 2508-2518.	13.8	92
27	Room-Temperature Reaction of Carbon Monoxide with a Stable Diarylgermylene. Journal of the American Chemical Society, 2009, 131, 6912-6913.	13.7	87
28	MnIII-enriched α-MnO2 nanowires as efficient bifunctional oxygen catalysts for rechargeable Zn-air batteries. Energy Storage Materials, 2019, 23, 252-260.	18.0	80
29	Defect Engineering of Palladium–Tin Nanowires Enables Efficient Electrocatalysts for Fuel Cell Reactions. Nano Letters, 2019, 19, 6894-6903.	9.1	79
30	An Unsymmetric Oxo/Imido-Bridged Germanium-Centered Singlet Diradicaloid. Journal of the American Chemical Society, 2009, 131, 14164-14165.	13.7	75
31	Electrochemical detection of Hg(II) ions based on nanoporous gold nanoparticles modified indium tin oxide electrode. Sensors and Actuators B: Chemical, 2015, 220, 1086-1090.	7.8	71
32	Activity and selectivity regulation through varying the size of cobalt active sites in photocatalytic CO ₂ reduction. Journal of Materials Chemistry A, 2018, 6, 21110-21119.	10.3	70
33	Elucidation of Active Sites on S, N Codoped Carbon Cubes Embedding Co–Fe Carbides toward Reversible Oxygen Conversion in Highâ€Performance Zinc–Air Batteries. Small, 2020, 16, e1907368.	10.0	66
34	Au-activated N motifs in non-coherent cupric porphyrin metal organic frameworks for promoting and stabilizing ethylene production. Nature Communications, 2022, 13, 63.	12.8	64
35	Selective Photocatalytic Reduction of CO ₂ to CH ₄ Modulated by Chloride Modification on Bi ₂ WO ₆ Nanosheets. ACS Applied Materials & Interfaces, 2020, 12, 54507-54516.	8.0	62
36	Dissecting the interfaces of MOF-coated CdS on synergized charge transfer for enhanced photocatalytic CO2 reduction. Journal of Catalysis, 2021, 397, 128-136.	6.2	61

YANG PENG

#	Article	IF	CITATIONS
37	Promoting ethylene production over a wide potential window on Cu crystallites induced and stabilized via current shock and charge delocalization. Nature Communications, 2021, 12, 6823.	12.8	61
38	Synthesis and Characterization of the Monomeric Sterically Encumbered Diaryls E{C6H3-2,6-(C6H3-2,6-Pri2)2}2 (E = Ge, Sn, or Pb). Zeitschrift Fur Anorganische Und Allgemeine Chemie, 2006, 632, 1005-1010.	1.2	58
39	Polypyrrole reinforced ZIF-67 with modulated facet exposure and billion-fold electrical conductivity enhancement towards robust photocatalytic CO2 reduction. Journal of Energy Chemistry, 2021, 60, 202-208.	12.9	56
40	Stabilizing and Activating Metastable Nickel Nanocrystals for Highly Efficient Hydrogen Evolution Electrocatalysis. ACS Nano, 2018, 12, 11625-11631.	14.6	55
41	Bandgap engineering of a lead-free defect perovskite Cs ₃ Bi ₂ I ₉ through trivalent doping of Ru ³⁺ . RSC Advances, 2018, 8, 25802-25807.	3.6	54
42	γ-Fe2O3 nanoparticles embedded in porous carbon fibers as binder-free anodes for high-performance lithium and sodium ion batteries. Journal of Alloys and Compounds, 2019, 777, 127-134.	5.5	52
43	Alkaliphilic Cu ₂ O nanowires on copper foam for hosting Li/Na as ultrastable alkali-metal anodes. Journal of Materials Chemistry A, 2019, 7, 20926-20935.	10.3	49
44	Boron-doped InSe monolayer as a promising electrocatalyst for nitrogen reduction into ammonia at ambient conditions. Applied Surface Science, 2019, 495, 143463.	6.1	46
45	Different reactivity of the heavier group 14 element alkyne analogues Ar′MMAr′ (M = Ge, Sn; Ar′ =) Tj ETÇ	2q110.78	4314 rgBT /
46	Bimetallic Fe-Ni phosphide carved nanoframes toward efficient overall water splitting and potassium-ion storage. Chemical Engineering Journal, 2020, 390, 124515.	12.7	45
47	Mosaic rGO layers on lithium metal anodes for the effective mediation of lithium plating and stripping. Journal of Materials Chemistry A, 2019, 7, 12214-12224.	10.3	44
48	A Doubleâ€Buffering Strategy to Boost the Lithium Storage of Botryoid MnO <i>_x</i> /C Anodes. Small, 2019, 15, e1900015.	10.0	42
49	Insulative Ion-Conducting Lithium Selenide as the Artificial Solid–Electrolyte Interface Enabling Heavy-Duty Lithium Metal Operations. Nano Letters, 2021, 21, 7354-7362.	9.1	42
50	Reversible complexation of isocyanides by the distannyne Ar′SnSnAr′ (Ar′ = C6H3-2,6(C6H3-2,6-iPr2)2). Chemical Communications, 2010, 46, 943.	4.1	40
51	Highly efficient water splitting driven by zinc-air batteries with a single catalyst incorporating rich active species. Applied Catalysis B: Environmental, 2020, 263, 118139.	20.2	38
52	Highâ€Performance Li–O ₂ Batteries Based on Allâ€Graphene Backbone. Advanced Functional Materials, 2020, 30, 2007218.	14.9	36
53	A "Blockchain―Synergy in Conductive Polymerâ€Filled Metal–Organic Frameworks for Dendriteâ€Free Li Plating/Stripping with High Coulombic Efficiency. Angewandte Chemie - International Edition, 2022, 61,	13.8	36
54	Crystal Splintering of β-MnO ₂ Induced by Interstitial Ru Doping Toward Reversible Oxygen Conversion. Chemistry of Materials, 2021, 33, 4135-4145.	6.7	34

#	Article	IF	CITATIONS
55	Construction of a ternary Z-scheme In2S3@Au@P3HT photocatalyst for the degradation of phenolic pollutants under visible light. Separation and Purification Technology, 2021, 272, 118787.	7.9	30
56	A hierarchical Single-Atom Ni-N3-C catalyst for electrochemical CO2 reduction to CO with Near-Unity faradaic efficiency in a broad potential range. Chemical Engineering Journal, 2022, 446, 137296.	12.7	30
57	Waxâ€Transferred Hydrophobic CVD Graphene Enables Waterâ€Resistant and Dendriteâ€Free Lithium Anode toward Long Cycle Li–Air Battery. Advanced Science, 2021, 8, e2100488.	11.2	28
58	Cobalt coordination with pyridines in sulfurized polyacrylonitrile cathodes to form conductive pathways and catalytic M-N4S sites for accelerated Li-S kinetics. Journal of Energy Chemistry, 2021, 61, 170-178.	12.9	28
59	Activating the MoS ₂ Basal Plane toward Enhanced Solar Hydrogen Generation via <i>in Situ</i> Photoelectrochemical Control. ACS Energy Letters, 2021, 6, 267-276.	17.4	27
60	Oxygen-vacancy-rich nickel hydroxide nanosheet: a multifunctional layer between Ir and Si toward enhanced solar hydrogen production in alkaline media. Energy and Environmental Science, 2022, 15, 3051-3061.	30.8	27
61	A Ditetrylyne as a l€-Electron Donor: Synthesis and Characterization of [AgArâ€2GeGeArâ€2] ⁺ SbF ₆ ^{â^{**}} and [Ag ₂ Arâ€2GeGe(F)Arâ€2] ⁺ SbF ₆ <6 ^{â^{**}} (Arâ€2 =) Tj ETQq1 1 0.7	84831.#4 rg	BT þ ðverlock
62	ĵournal of the American chemical Society, 2010, 1927, 19190 (1919). Î ³ -Fe2O3 nanoparticles aligned in porous carbon nanofibers towards long life-span lithium ion batteries. Electrochimica Acta, 2018, 289, 264-271.	5.2	25
63	Redox-Driven Lithium Perfusion to Fabricate Li@Ni–Foam Composites for High Lithium-Loading 3D Anodes. ACS Applied Materials & Interfaces, 2020, 12, 9355-9364.	8.0	24
64	Selfâ€Phosphorization of MOFâ€Armored Microbes for Advanced Energy Storage. Small, 2020, 16, e2000755.	10.0	23
65	Syntheses and Structures of Layered Copper(II) Diphosphonates with Mixed Ligands. European Journal of Inorganic Chemistry, 2003, 2003, 726-730.	2.0	22
66	Synthesis and Characterization of Two of the Three Isomers of a Germaniumâ€5ubstituted Bicyclo[2.2.0]hexane Diradicaloid: Stretching the GeGe Bond. Angewandte Chemie - International Edition, 2010, 49, 4593-4597.	13.8	22
67	Chemically Exfoliated Semiconducting Bimetallic Porphyrinylphosphonate Metal–Organic Layers for Photocatalytic CO ₂ Reduction under Visible Light. ACS Applied Energy Materials, 2021, 4, 4319-4326.	5.1	22
68	Unpaired 3d Electrons on Atomically Dispersed Cobalt Centres in Coordination Polymers Regulate both Oxygen Reduction Reaction (ORR) Activity and Selectivity for Use in Zinc–Air Batteries. Angewandte Chemie, 2020, 132, 292-300.	2.0	21
69	rGO-CNT aerogel embedding iron phosphide nanocubes for high-performance Li-polysulfide batteries. Carbon, 2020, 167, 446-454.	10.3	21
70	Nitrogen-doped carbon fibers embedding CoO _x nanoframes towards wearable energy storage. Nanoscale, 2020, 12, 8922-8933.	5.6	19
71	Steering the Pathway of Plasmonâ€Enhanced Photoelectrochemical CO ₂ Reduction by Bridging Si and Au Nanoparticles through a TiO ₂ Interlayer. Small, 2022, 18, e2201882.	10.0	19
72	Combining Multivariate Electrospinning with Surface MOF Functionalization to Construct Tunable Active Sites toward Trifunctional Electrocatalysis. Small, 2022, 18, e2106260.	10.0	18

#	Article	IF	CITATIONS
73	Robust photocatalytic hydrogen production on metal-organic layers of Al-TCPP with ultrahigh turnover numbers. Chinese Chemical Letters, 2021, 32, 3833-3836.	9.0	17
74	Homogenizing Li ₂ CO ₃ Nucleation and Growth through High-Density Single-Atomic Ru Loading toward Reversible Li-CO ₂ Reaction. ACS Applied Materials & Interfaces, 2022, 14, 18561-18569.	8.0	17
75	AgAuPt nanocages for highly sensitive detection of hydrogen peroxide. RSC Advances, 2015, 5, 7854-7859.	3.6	16
76	Revisiting the Grain and Valence Effect of Oxide-Derived Copper on Electrocatalytic CO ₂ Reduction Using Single Crystal Cu(111) Foils. Journal of Physical Chemistry Letters, 2021, 12, 3941-3950.	4.6	16
77	Polyacrylonitrile-based gel polymer electrolyte filled with Prussian blue forhigh-performance lithium polymer batteries. Chinese Chemical Letters, 2021, 32, 890-894.	9.0	15
78	Breaking the Linear Scaling Relationship by Compositional and Structural Crafting of Ternary Cu–Au/Ag Nanoframes for Electrocatalytic Ethylene Production. Angewandte Chemie, 2021, 133, 2538-2548.	2.0	15
79	Wax-assisted crack-free transfer of monolayer CVD graphene: Extending from standalone to supported copper substrates. Applied Surface Science, 2019, 493, 81-86.	6.1	14
80	Effect of Binder Conformity on the Electrochemical Behavior of Graphite Anodes with Different Particle Shapes. Wuli Huaxue Xuebao/ Acta Physico - Chimica Sinica, 2019, 35, 1382-1390.	4.9	14
81	Freestanding Electrode Pairs with High Areal Density Fabricated under High Pressure and High Temperature for Flexible Lithium Ion Batteries. ACS Applied Energy Materials, 2018, 1, 3171-3179.	5.1	13
82	Photoluminescent WSe2 nanofibers as freestanding cathode for Solar-assisted Li-O2 battery with ultrahigh capacity and transparent casing. Chemical Engineering Journal, 2022, 448, 137591.	12.7	13
83	Ru-Embedded Highly Porous Carbon Nanocubes Derived from Metal–Organic Frameworks for Catalyzing Reversible Li ₂ O ₂ Formation. ACS Applied Materials & Interfaces, 2021, 13, 28295-28303.	8.0	12
84	Rational design and mass-scale synthesis of guar-derived bifunctional oxygen catalyst for rechargeable Zn-air battery with active sites validation. Chemical Engineering Journal, 2022, 428, 131225.	12.7	12
85	Synthesis and thermolytic behavior of tin(iv) formates: in search of recyclable metal–hydride systems. Dalton Transactions, 2010, 39, 10659.	3.3	11
86	Copper-based Conductive Metal Organic Framework <i>In-situ</i> Grown on Copper Foam as a Bifunctional Electrocatalyst. Wuli Huaxue Xuebao/ Acta Physico - Chimica Sinica, 2019, 35, 1404-1411.	4.9	11
87	Structural and interfacial engineering of well-defined metal-organic ensembles for electrocatalytic carbon dioxide reduction. Chinese Journal of Catalysis, 2022, 43, 1417-1432.	14.0	11
88	In Situ Constructed P–N Junction on Cu ₂ O Nanocubes through Reticular Chemistry for Simultaneously Boosting CO ₂ Reduction Depth and Ameliorating Photocorrosion. Advanced Energy and Sustainability Research, 2022, 3, 2100134.	5.8	9
89	Gradient‣tructuring Manipulation in Ni ₃ S ₂ Layer Boosts Solar Hydrogen Production of Si Photocathode in Alkaline Media. Advanced Energy Materials, 2022, 12, .	19.5	9
90	Fast-charging and dendrite-free lithium metal anode enabled by partial lithiation of graphene aerogel. Nano Research, 2022, 15, 9792-9799.	10.4	8

#	Article	IF	CITATIONS
91	Active nickel derived from coordination complex with weak inter/intra-molecular interactions for efficient hydrogen evolution via a tandem mechanism. Journal of Catalysis, 2020, 389, 29-37.	6.2	7
92	K[Al ₄ (PPh ₂) ₇ PPh]: An Al ^{II} Phosphanide / Phosphinidene Intermediate on the Path to AlP Formation. Zeitschrift Fur Anorganische Und Allgemeine Chemie, 2013, 639, 2558-2560.	1.2	6
93	One-dimensional HKUST-1 nanobelts from Cu nanowires. Chinese Chemical Letters, 2020, 31, 517-520.	9.0	6
94	Entrapping polysulfides via S, N-coordinated supermolecule towards enhanced Li-S kinetics. Chemical Engineering Journal, 2021, 426, 131355.	12.7	6
95	Cupric porphyrin frameworks on multi-junction silicon photocathodes to expedite the kinetics of CO ₂ turnover. Nanoscale, 2022, 14, 8906-8913.	5.6	6
96	Design of experiments unravels insights into selective ethylene or methane production on evaporated Cu catalysts. Journal of Energy Chemistry, 2022, 75, 422-429.	12.9	6
97	Fabrication of nanoporous AuPt nanoparticles modified indium tin oxide electrode and their electrocatalytic effect. Ionics, 2017, 23, 1203-1208.	2.4	5
98	Progress on the Development of Inorganic Lead-Free Perovskite Solar Cells. Wuli Huaxue Xuebao/ Acta Physico - Chimica Sinica, 2017, 33, 1379-1389.	4.9	5
99	A "Blockchain―Synergy in Conductive Polymerâ€Filled Metal–Organic Frameworks for Dendriteâ€Free Li Plating/Stripping with High Coulombic Efficiency. Angewandte Chemie, 2022, 134, .	2.0	5
100	Aluminium(III) amidinates formed from reactions of `AlCl' with lithium amidinates. Acta Crystallographica Section C: Crystal Structure Communications, 2013, 69, 1120-1123.	0.4	3
101	Tetrabromidobis(dicyclohexylphosphane-κP)digallium(Ga—Ga). Acta Crystallographica Section E: Structure Reports Online, 2012, 68, m1245-m1245.	0.2	2
102	Controllable Electrochemical Synthesis of Silver Nanoparticles on Indiumâ€Tinâ€Oxideâ€Coated Glass. ChemElectroChem, 2015, 2, 578-583.	3.4	2
103	Bis[tris(ethylenediamine)cobalt(III)] dichlorobis[μ-(1-hydroxyethylidene)diphosphonato(4–)]diruthenium(II,III)(Ru–Ru) chloride trihydrate. Acta Crystallographica Section C: Crystal Structure Communications, 2004, 60, m302-m304.	0.4	1